Nanoscale

COMMUNICATION

View Article Online
View Journal

Cite this: DOI: 10.1039/d2nr05732h

Received 15th October 2022,
Accepted 10th February 2023

DOI: 10.1039/d2nr05732h

rsc.li/nanoscale

Investigation of local distortion effects on X-ray absorption of ferroelectric perovskites from first principles simulations†

Pedram Abbasi, David P. Fenning and Tod A. Pascal *

Understanding the role of ferroelectric polarization in modulating the electronic and structural properties of crystals is critical for advancing these materials for overcoming various technological and scientific challenges. However, due to difficulties in performing experimental methods with the required resolution, or in interpreting the results of methods therein, the nanoscale morphology and response of these surfaces to external electric fields has not been properly elaborated. In this work we investigate the effect of ferroelectric polarization and local distortions in a $BaTiO_3$ perovskite, using two widely used computational approaches which treat the many-body nature of X-ray excitations using different philosophies, namely the many-body, delta-self-consistent-field determinant (mb-ΔSCF) and the Bethe–Salpeter equation (BSE) approaches. We show that in agreement with our experiments, both approaches consistently predict higher excitations of the main peak in the O–K edge for the surface with upward polarization. However, the mb-ΔSCF approach mostly fails to capture the $L_{2,3}$ separations at the Ti–L edge, due to the absence of spin–orbit coupling in Kohn–Sham density functional theory (KS-DFT) at the generalized gradient approximation level. On the other hand, and most promising, we show that application of the GW/BSE approach successfully reproduces the experimental XAS, both the relative peak intensities as well as the $L_{2,3}$ separations at the Ti–L edges upon ferroelectric switching. Thus simulated XAS is shown to be a powerful method for capturing the nanoscale structure of complex materials, and we underscore the need for many-body perturbation approaches, with explicit consideration of core-hole and multiplet effects, for capturing the essential physics in these systems.

Department of Nano and Chemical Engineering, University of California San Diego, La Jolla, CA 92093, USA. E-mail: tpascal@ucsd.edu

†Electronic supplementary information (ESI) available: Additional details on experimental and computational methods. Input files, pseudopotentials and other relevant files for performing ΔSCF (MBXAS) and GW-BSE (Ocean) calculations have been deposited to the following repository: **https://github.com/atlas-nano/Computational_XAS**. See DOI: **https://doi.org/10.1039/d2nr05732h**

Tod A. Pascal

Prof. Tod A. Pascal is an Assistant Professor of Nano Engineering and Chemical Engineering; affiliate faculty of Materials Science and Engineering and the Sustainable Power and Energy Center, and a lead investigator for the UC San Diego MRSEC. Prof. Pascal's research group advances theoretical and computational methods to elucidate the structure and dynamics of electro-chemical systems, disorder in condensed phase systems and spectroscopy at molecular interfaces.

Introduction

Utilization of ferroelectrics in a wide range of electronic and energy conversion devices during the past decades has spurred ever extensive research on the structural and electronic properties of this class of materials.[1,2] A wide range of ferroelectrics belong to the perovskite family, with a general structure of ABO_3, where significant and controlled modulation of the bulk and surface properties, upon polarization switching, has been observed.[3,4] This includes the reversible change in surface structure and electronic charge density, relevant to applications ranging from sensors and non-volatile memories.[5,6] The chemistry of ferroelectric perovskites mainly consist of titanates ($ATiO_3$) in which the A site is a cation such as Pb,[2] Sr,[7] Ba,[8] Ca[9] or Li.[7] Here, ferroelectricity originates from the displacement of Ti^{4+} cations from their centrosymmetric positions to two meta-stable configurations, with positive and negative polarizations.[10] It is now well established that this effect originates from Ti–O bonding and orbital

hybridization, and that a deep understanding of electronic structure is necessary to elucidate the effect of polarization switching in ABO_3 perovskites.[9,11]

To date, various spectroscopic methods have been developed to probe the role of polarization on the overall properties of ferroelectrics, in both solid state and molecular systems.[12–19] Among them, X-ray absorption spectroscopy (XAS) is a unique and powerful tool that is capable of probing the electronic structure of selected elements with high sensitivity to the local structure and short-range interactions, critical for understanding the effect of ferroelectric polarization on surface local electronic structure and chemistry. XAS fundamentally relies on excitations of core electrons to unoccupied valence states *i.e.*, transition metal 2p and 3d orbitals, corresponding to O–K and Ti–L edges respectively.[20] Specifically, O–K (1s → 2p) excitations has been widely studied, both experimentally and computationally, to shed light on surface and interface originating properties of ferroelectrics, such as surface charge density and relaxation.[20–22] However there is still a lack of understanding on the direct role of polarization switching (and the associated changes in dipole moment) on the O–K edge fine structure. Ti–L edge transitions (2p → 3d) involve even more complex physics, including interatomic spin–orbit coupling and strong multiplet effects.[20,23,24] This has made polarization switching studies at the Ti–L edge more challenging.

For a comprehensive understanding of quantum-chemical methods on X-ray absorption and their relevance to different systems, we refer to recent reviews.[25,26] We here summarize efficient computational approaches for simulating the XAS of complex material systems, such as the perovskites considered here. These range from band structure multiplet approaches,[25,27] time-dependent density-functional theory (TDDFT),[28,29] multiple-scattering,[30–32] and application of the Bethe–Salpeter equation (BSE) in second-order perturbation theory approaches.[25,33] In general, these methods can be classified into two categories, based on how the XAS final states are modelled: (i) single-particle and (ii) many-body approaches.[26,34]

In single-particle excitation approaches, the excited electron and its corresponding hole are treated as independent particles, (sometimes modelled as impurities),[26,34] the system's electron density is equilibrated in its final (core-excited) state and the XAS spectrum generated by calculating transition matrix probabilities from the overlap of the initial (ground) and final states. The most widely used method is based on constrained-occupancy delta-self-consistent-field (ΔSCF) DFT, in which transition amplitudes are calculated based on a fixed core-hole potential. Based on this general approach, various computational schemes have been developed, which mostly differ in whether or not the X-ray photo-electron is included in the final state, as in the so-called excited-electron and core-hole (XCH) or full core-hole (FCH) approaches, respectively.[34]

One can of course go beyond single-particle interactions and solve the electron–hole interactions within many-body perturbation theory. Here, the final state is assumed to be a superposition of effective e–h pairs. One way of accomplishing this is by solving the Bethe–Salpeter Equation (BSE) equation, which includes quasi-particle energies of the core hole and the excited photoelectron, together with the interaction between them.[23,35] Since capturing the effect of lattice distortion at the atomic scale in transition metals and perovskite crystals involves multiple, many-electron effects, methods based on many-body interactions are thought critical in accurately capturing the physics of the experimental system. However, this has not been comprehensively explored.

In this work, we seek to answer two equally important questions about the surface and electronic structure of polarized $BaTiO_3$ slabs. First, we investigate the role of polarization switching in modulating the surface electronic states, using both experiments and first principles based simulated XAS at the O–K and Ti–L edges, on upward and downward polarized, epitaxially grown (001) thin films. Secondly, we benchmark the performance of two approaches for including many-body physics in the XAS: a many-body ΔSCF determinant approach, and a hybrid GW/BSE approach based on many-body perturbation theory. These are herein denoted the determinant and BSE approaches, respectively. By benchmarking against experimental data,[36] we show that while both approaches accurately predict the effect of ferroelectric modulation on the main edges and fine structures at the O–K edge, *i.e.*, low energy t_{2g} peaks, the consideration of multiplet and spin–orbit coupling effects is critical for accurately capturing the physics, and is necessary to model 2p → 3d transitions associated with Ti–L edges.

Results

Fig. 1a shows the TiO_6 octahedron in the $BaTiO_3$ tetragonal structure, with a Ti atom at the center and 6 O atoms on each corner. In titanate perovskites, the crystal ligand field on the Ti-3d electrons creates low energy and high energy sub-bands, known as t_{2g} and e_g, as shown in Fig. 1b.[22] Direct hybridization between the Ti-3d and O-2p electrons in the TiO_6 octahedron leads to the formation of d_{z^2} and $d_{x^2-y^2}$ orbitals (corresponding to e_g peaks), while their in-plane hybridization leads to d_{xy}, d_{xz} or d_{yz} orbitals (attributed to t_{2g} states).[37,38] Fig. 1c and e shows the surface-sensitive experimental Ti–L and O–K XAS of $BaTiO_3$ thin films, collected by synchrotron X-ray scanning tunneling microscopy (SX-STM).[39–41] Tunneling of photo-excited electrons to the STM tip in the near-field mode allows us to capture surface polarization switching effects with high sensitivity. Analysis of the resulting spectra shows that the Ti–L XAS is characterized by two pairs of peaks, at 456.4 eV and 458.53 eV and at 461.93 eV and 464.06 eV, associated with t_{2g} and e_g orbitals at the L_3 and L_2 states respectively. Corresponding t_{2g} and e_g fine structure features at the O–K are observed at 529.65 V and 532.1 eV. Overall, we find that switching the polarization from downward to upward leads to a reproducible and prominent increase in the peak intensity ratios of the t_{2g} and e_g states denoted as (P^+/P^+). Specifically, we find that the relative

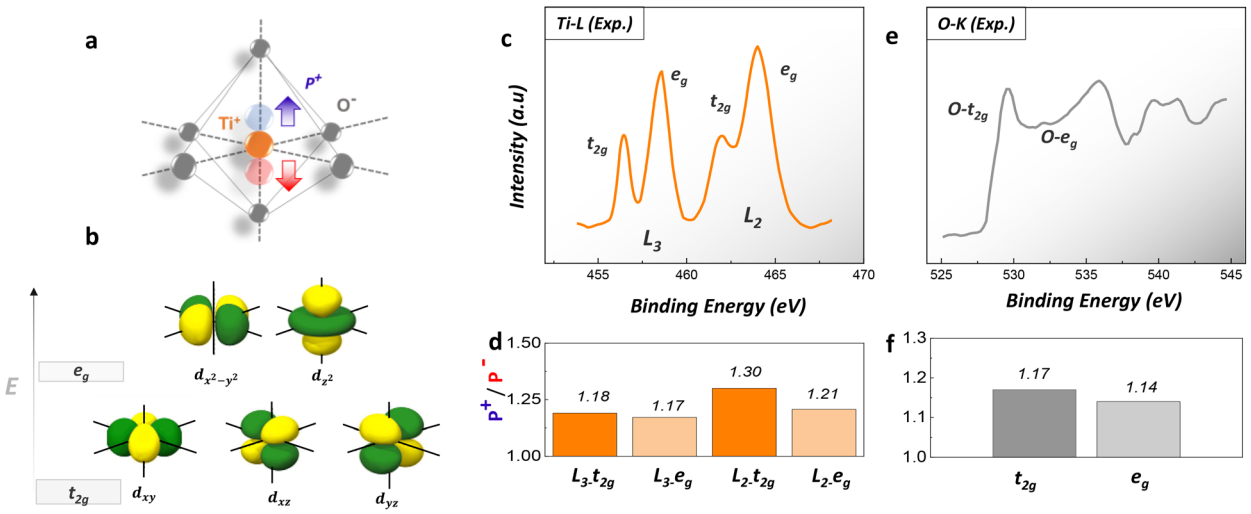

Fig. 1 (a) Schematic TiO_6 octahedron within the $BaTiO_3$ tetragonal structure, with a Ti^+ cation in upward (blue) and downward (red) polarization states (b) possible hybridized orbitals between Ti-d and O-p states with d_{z^2} and $d_{x^2-y^2}$ on e_g and d_{xy}, d_{xz} or d_{yz} orbitals on t_{2g} states. Experimental XAS spectra and corresponding intensity ratios on each peak in upward *vs.* downward positions on (c and d) Ti–L and (e and f) O–K edges of epitaxial $BaTiO_3$.

intensity of the t_{2g} and e_g peaks in upward and downward polarized surfaces confirms is most sensitive at the Ti–L_2 edge (Fig. 1c and d), in agreement with previous reports showing a high sensitivity of the low energy fine structures of Ti–L and O–K to lattice distortion.[38]

Fig. 2 presents the simulated O–K edge XAS spectra of $BaTiO_3$, based on the multi-determinant ΔSCF approach. A schematic describing the excitation of core electrons to valence band empty states, with the associated, many-body, first and second order valence excitations is shown in the schematic in Fig. 2a. Here the excitation order (f^a) denotes the number of e–h pairs considered for simulating the determinant spectrum (*i.e.*, f^2 represents two sets of e–h pairs). The effect of the total number of empty orbitals in valence band $(n \times m)$ is also considered, where m is the number of occupied orbitals in the ground state. Ideally to resemble a many-body effect one should consider a complete picture of valence excitations and multi-scattering effects (*i.e.*, f^a excitation orders), however recent experience has shown that for early transition metal oxides, spectra converges at a low valence excitation order.[34] We verified this in the current context by first calculating the determinant spectrums for O–K excitations with different number of empty orbitals in valence band, and found that we achieved convergence in the spectra (up to 20 eV above the adsorption edge) at $n = 3$. We also investigated the effect of the excitation order, by considering single (f^1), and double e–h pairs (f^2). This also showed that converged was achieved with second order excitation (Fig. 2c). The determinant spectrum,

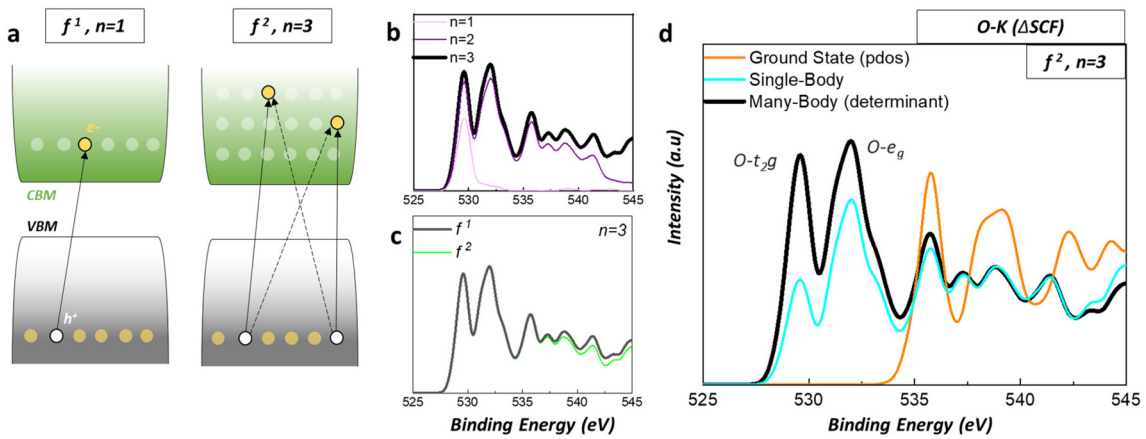

Fig. 2 Excitation principles within many-body perturbation model. (a) Schematic of possible excitations from conduction band to valence band with first and second excitation order. (b) The effect of number of empty orbitals in valence band and (c) excitation order on determinant final spectrum. (d) Initial (ground) state, one body excited state and determinant spectrum.

based on double e–h pairs, mainly affected higher energy peaks, and had no appreciable effect on the main e_g and t_{2g} fine structures.[34]

As a figure of merit, we also calculated the spectrum using the initial state approximation, which amounts to a projected density of states (pDOS) calculation. We compare this to the single-particle final-state spectrum and the spectrum based on determinant approach at the O–K edge in Fig. 1d. This shows conclusively that the multi-determinant approach is necessary to accurately capture the physics in these systems. Notably, in Fig. 2d, we calculate a red shift of ~7 eV when comparing the pDOS to the multi-determinant spectrum, with the former completely missing the critical t_{2g} and e_g features. Further, the single-particle XAS approach fails to capture the main low energy t_{2g} fine structure and to reproduce the experimental t_{2g}/e_g ratio. By contrast, the many-body determinant approach substantially improves the intensity of the main t_{2g} peak, compared with experiments.

We further investigated the effect of local ferroelectric polarization on both the Ti–L and O–K edge spectra, simulated using the converged (f^2 and $n = 3$) determinant approach, with polarized slab models (Fig. 3). To fully elucidate the signature of local polarization on the electronic structure of the slab, we investigated two degrees of local distortion of Ti from its centrosymmetric position, namely P_1 and P_2, corresponding to polarizations of ~18 μC cm^{-2} and ~32 μC cm^{-2}, respectively [see ESI for more details†]. The resulting O–K edge XAS spectra shows the characteristic t_{2g} and e_g peaks at 529.3 eV and 532.0 eV, and an increase in the peak intensity when switching the polarization from downward (P^-) to upward (P^+) in line with our experimental findings. Indeed, we find that the P^+/P^- ratio (denoted on each peak in *italics*) for both the t_{2g} and e_g peaks intensifies with increasing distortion (*i.e.*, going from P_1 to P_2), confirming that the peak modulations do indeed originated from local polarization.

Next, we investigated the performance of the determinant approach in capturing Ti–L edge excitations on our polarized slab models. As can be seen in Fig. 3d and e, we are only able to reproduce the pair of peaks at 456.3 eV and 458.4 eV, associated with low energy L_3 states of $BaTiO_3$. In other words, the multi-determinant approach fails to capture the L_2 peaks, due to problems in properly describing the crystal-field effect, and specifically the lack of consideration of the splitting of the d states due to multiplet effects.[42] Moreover, for the L_3 peaks, we find that the relative t_{2g}/e_g ratio of ~1.9 is reversed compared with the experimental value of ~0.55. However, while the determinant approach fails to capture any L_2 peaks, we find that it is still capable capturing some essential physics in these systems. Namely, we calculate a P^+/P^- >1 at both the L_3 t_{2g} and e_g peaks, which further intensifies when increasing the extent of polarization from P_1 to P_2, consistent with our experimental findings.

It is well appreciated that the simulated XAS spectrum of complex materials, including transition-metal oxides, can be

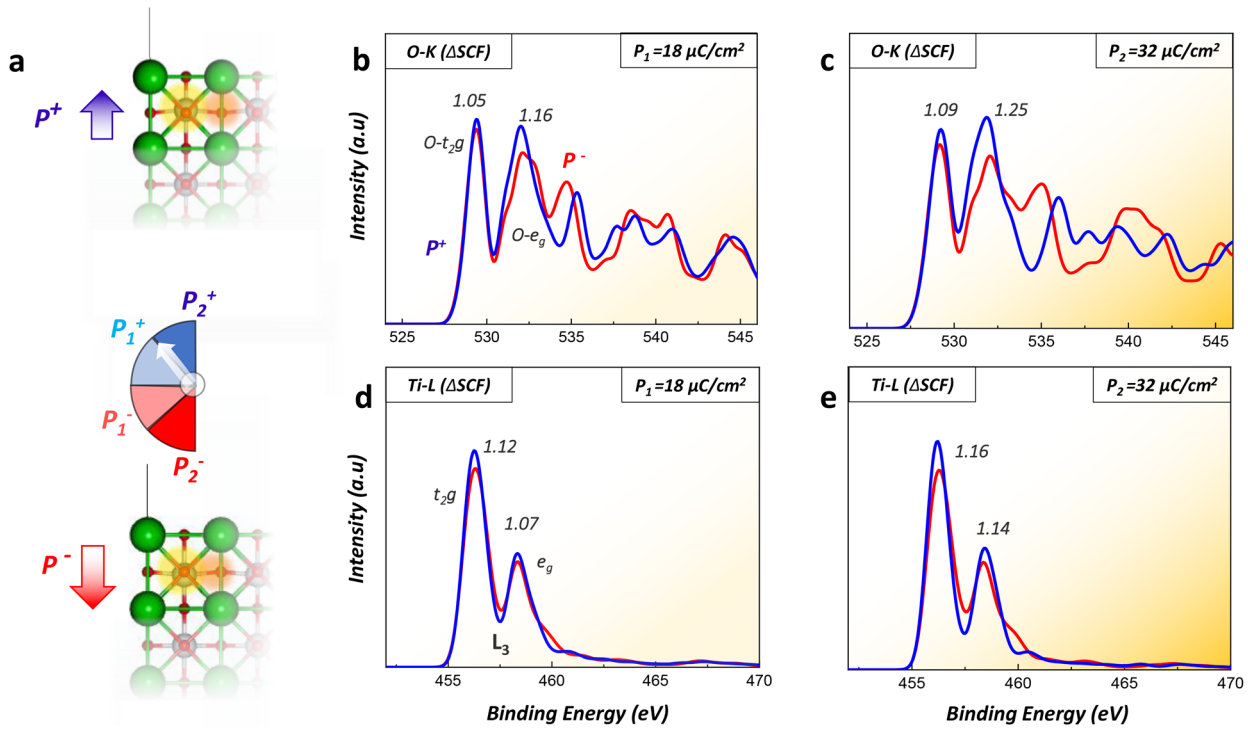

Fig. 3 Excitations based on many-body, determinant ΔSCF approach. (a) schematic of $BaTiO_3$ polarized slabs with upward and downward polarizations (b and c) O–K edge with t_{2g} and e_g peaks labeled with P_1 and P_2 polarization extent (d and e) Ti–L edge with t_{2g} and e_g peaks labeled with P_1 and P_2 polarization extent. Relative peak intensities between upward and downward polarized models (P^+/P^-) is noted on each peak.

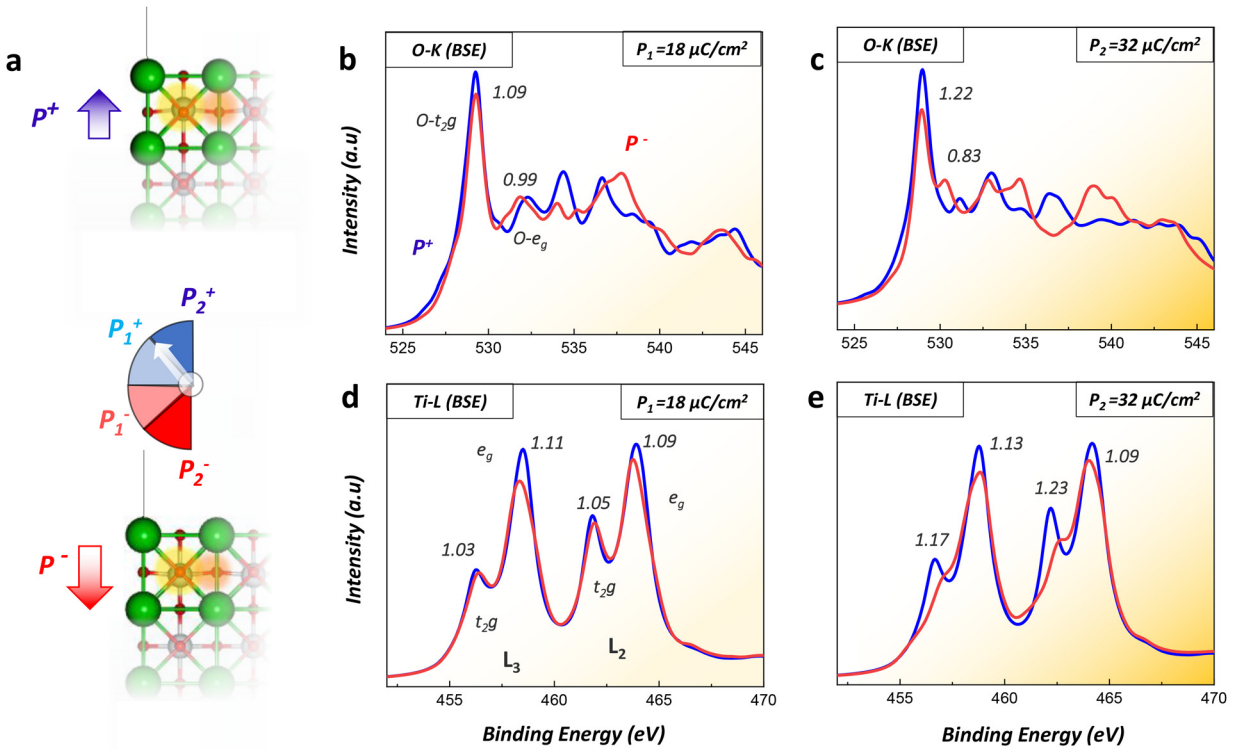

Fig. 4 Excitations based on BSE approach. (a) schematic of $BaTiO_3$ polarized slabs with upward and downward polarizations (b and c) O–K edge with t_{2g} and e_g peaks labeled with P_1 and P_2 polarization extent (d and e) Ti–L edge with t_{2g} and e_g peaks labeled with P_1 and P_2 polarization extent. Relative peak intensities between upward and downward polarized models (P^+/P^-) is noted on each peak in italic.

significantly improved by inclusion of more complex e–h pair screening and exciton-binding physics. We quantify this in the current context by presenting the O–K and Ti–L edge spectra, based on the many-body GW/BSE approach in Fig. 4. We find that the corresponding O–K spectra, presented in Fig. 4b and c, shows a significant increase on the intensity of low energy t_{2g} peak compared with determinant approach, and more in line with our experimental data. Moreover, the effect of polarization switching is also more apparent using the BSE approach, as demonstrated by the sharp increase in intensity for the poled-up surface compared with poled down surface. Increasing the distortion and polarization from P_1 to P_2 leads to a larger difference on the intensity of t_{2g} peak between poled up and poled down, again confirming that the change in electronic structure originates from polarization switching. The characteristic t_{2g} and e_g peaks under P_1 polarization are observed at 529.2 eV and 532.2 eV while a higher level of distortion due to increased polarization (*i.e.*, P_2 *vs.* P_1) blue shifts the position of e_g peak ~1 eV, while we find that the line shape of the higher energy peaks are further modulated, which can be attributed to the presence of multi-scattering effects.

The simulated XAS at the Ti–L edge using the BSE approach is shown in Fig. 4d and e. Here, and in contrast to the multi-determinant ΔSCF approach, we find a total of four sharp peaks: at 456.3 eV, 458.5 eV attributed to L_3 and at 461.8 eV and 463.9 eV attributed to the L_2 t_{2g} and e_g states, respectively. In addition to capturing both L_2 features, we find that the BSE approach better represents the t_{2g}/e_g ratio for the L_2 and L_3 peaks, compared to the experiments. We also find that increasing the polarization, from P_1 to P_2, leads to the most pronounced effect on the t_{2g} peak of Ti–L spectra, also in better agreement with experiments compared to the multi determinant ΔSCF approach. Thus, the significantly improved physics in BSE, which captures the spin–orbit coupling effect, produces a much-improved XAS spectrum.

Conclusion

In this work we investigated the effect of lattice distortion and polarization switching on the X-ray absorption at the Ti–L and O–K edges of a ferroelectric $BaTiO_3$ film, experimentally and computationally using two advanced approaches. We find that the multi-determinant computational approach improves on the more widely used single-particle electron–hole method, and leads to a better t_{2g}/e_g ratio at the O–K edge, while reproducing the higher intensity excitations for poled up surface observed in experiments. This approach fails however to reproduce the observed $L_{2,3}$ separation, due to the lack of spin–orbit coupling at the Ti–L edge. In comparison, the many-body BSE approach better captures both the near edge fine structures at the O–K edge and reproduces the $L_{2,3}$ separation and the t_{2g}/e_g ratios observed experimentally. Thus, the inclusion of both spin–orbit coupling and the superior electron–hole screening

and photoexcitation dynamics in BSE is critical from simulating the XAS in this class of materials and also in other systems with strong spin-coupling effects *i.e.* 4d and 5d transition metals. Accessing and quantifying the performance of first principle spectroscopic methods, tailored toward specific physical models, is necessary for future studies aimed at using these approaches as independent and complementary probes for studying the structural and electronic properties of these complex systems.

Author contributions

P. A. performed *ab initio* electronic structure and computational XAS calculations. D. P. F. and T. A. P. supervised experimental and computational efforts. All the authors contributed to the manuscript.

Conflicts of interest

The authors declare no competing financial interests.

Acknowledgements

This research was primarily supported by the NSF through the UC San Diego Materials Research Science and Engineering Center (UCSD MRSEC), Grant No. DMR-2011924. T. A. P. and D. P. F. acknowledge startup funding from the Jacob school of Engineering, UCSD. T. A. P. acknowledges additional support from the NSF through a CAREER award, Grant No. CBET-309147, and the US DOE, Grant No. BES-311015. This work used the computational resources from the Extreme Science and Engineering Discovery Environment (XSEDE) and the Expanse supercomputer at the San Diego Super Computing Center (SDSC), through allocation CSD622 and DDP381. The authors thank S. Jamnuch and D. G. Prendergast for helpful discussions on XAS calculations. Also, we are thankful to N. Shirato and V. Rose at Argonne National Lab for assistance on collecting the experimental data sets.

References

1 J. F. Scott, Applications of Modern Ferroelectrics, *Science*, 2007, **315**(5814), 954–959, DOI: **10.1126/science.1129564**.

2 R. E. Cohen, Origin of Ferroelectricity in Perovskite Oxides, *Nature*, 1992, **358**(6382), 136–138, DOI: **10.1038/358136a0**.

3 K. Mistewicz, Recent Advances in Ferroelectric Nanosensors: Toward Sensitive Detection of Gas, Mechanothermal Signals, and Radiation, *J. Nanomater.*, 2018, **2018**, 1–15, DOI: **10.1155/2018/2651056**.

4 D. G. Popescu, N. Barrett, C. Chirila, I. Pasuk and M. A. Husanu, Influence of Hole Depletion and Depolarizing Field on the BaTiO3/La0.6Sr0.4MnO3 Interface Electronic Structure Revealed by Photoelectron Spectroscopy and First-Principles Calculations, *Phys. Rev. B: Condens. Matter Mater. Phys.*, 2015, **92**(23), 0–11, DOI: **10.1103/PhysRevB.92.235442**.

5 P. Abbasi, M. R. Barone, M. de la Paz Cruz-Jáuregui, D. Valdespino-Padilla, H. Paik, T. Kim, L. Kornblum, D. G. Schlom, T. A. Pascal and D. P. Fenning, Ferroelectric Modulation of Surface Electronic States in BaTiO 3 for Enhanced Hydrogen Evolution Activity, *Nano Lett.*, 2022, **22**(10), 4276–4284, DOI: **10.1021/acs.nanolett.2c00047**.

6 P. Abbasi, D. P. Fenning and T. A. Pascal, Electrocatalytic Hydrogen Evolution on Ferroelectric Perovskite Heterostructures, *ECS Meet. Abstr.*, 2022, **MA202201**(38), 1691–1691, DOI: **10.1149/MA2022-01381691mtgabs**.

7 R. I. Eglitis, Ab Initio Calculations of SrTiO3, BaTiO3, PbTiO 3, CaTiO3, SrZrO3, PbZrO3 and BaZrO3 (001), (011) and (111) Surfaces as Well as F Centers, Polarons, KTN Solid Solutions and Nb Impurities Therein, *Int. J. Mod. Phys. B*, 2014, **28**(17), 1430009-1–1430009-43, DOI: **10.1142/S0217979214300096**.

8 C. Ederer and N. A. Spaldin, Effect of Epitaxial Strain on the Spontaneous Polarization of Thin Film Ferroelectrics, *Phys. Rev. Lett.*, 2005, **9**(25), 257601–257604, DOI: **10.1103/PhysRevLett.95.257601**.

9 G. Z. Wang, C. R. Li, J. Cuib and Z. Y. Manc, Ab Initio Study of ATiO3(001) Surfaces, *Surf. Interface Anal.*, 2009, **41**(12–13), 918–923, DOI: **10.1002/sia.3119**.

10 K. M. Rabe, C. H. Ahn, J. M.-M. Triscone, M. Dawber and C. Lichtensteiger, Physics of Ferroelectrics, in *Topics in Applied Physics*, Springer Berlin Heidelberg, Berlin, Heidelberg, 2007, vol. 105. DOI: **10.1007/978-3-540-34591-6**.

11 M. Zhong, W. Zeng, F. S. Liu, B. Tang and Q. J. Liu, First-Principles Study of the Atomic Structures, Electronic Properties, and Surface Stability of BaTiO3 (001) and (011) Surfaces, *Surf. Interface Anal.*, 2019, 1021–1032, DOI: **10.1002/sia.6688**.

12 B. C. Huang, Y. T. Chen, Y. P. Chiu, Y. C. Huang, J. C. Yang, Y. C. Chen and Y. H. Chu, Direct Observation of Ferroelectric Polarization-Modulated Band Bending at Oxide Interfaces, *Appl. Phys. Lett.*, 2012, **100**(12), 122903–122906, DOI: **10.1063/1.3691615**.

13 N. Barrett, J. Rault, I. Krug, B. Vilquin, G. Niu, B. Gautier, D. Albertini, P. Lecoeur and O. Renault, Influence of the Ferroelectric Polarization on the Electronic Structure of BaTiO3 Thin Films, *Surf. Interface Anal.*, 2010, **42**(12–13), 1690–1694, DOI: **10.1002/sia.3369**.

14 J. L. Wang, A. Pancotti, P. Jégou, G. Niu, B. Gautier, Y. Y. Mi, L. Tortech, S. Yin, B. Vilquin and N. Barrett, Ferroelectricity in a Quasiamorphous Ultrathin BaTiO3 Film, *Phys. Rev. B: Condens. Matter Mater. Phys.*, 2011, **84**(20), 205426-1–205426-7, DOI: **10.1103/PhysRevB.84.205426**.

15 D. A. Tenne, A. Bruchhausen, N. D. Lanzillotti-Kimura, A. Fainstein, R. S. Katiyar, A. Cantarero, A. Soukiassian, V. Vaithyanathan, J. H. Haeni, W. Tian, D. G. Schlom, K. J. Choi, D. M. Kim, C. B. Eom, H. P. Sun, X. Q. Pan, Y. L. Li, L. Q. Chen, Q. X. Jia, S. M. Nakhmanson,

K. M. Rabe and X. X. Xi, Probing Nanoscale Ferroelectricity by Ultraviolet Raman Spectroscopy, *Science*, 2006, **313**(5793), 1614–1616, DOI: 10.1126/science.1130306.

16 J. L. Wang, B. Vilquin and N. Barrett, Screening of Ferroelectric Domains on BaTiO 3(001) Surface by Ultraviolet Photo-Induced Charge and Dissociative Water Adsorption, *Appl. Phys. Lett.*, 2012, **101**(9), 2012–2015, DOI: 10.1063/1.4748330.

17 J.-G. Zheng, T. Aoki and A. Paul, TEM Study of Epitaxial LSMO-BTO-STO Thin Film Heterostructures, *Microsc. Microanal.*, 2018, **24**(S1), 2028–2029, DOI: 10.1017/s1431927618010620.

18 H. Chang, N. Shirato, Y. Zhang, J. Hoffman, D. Rosenmann, J. W. Freeland, A. Bhattacharya, V. Rose and S. W. Hla, X-Ray Magnetic Circular Dichroism and, near-Edge X-Ray Absorption Fine Structure of Buried Interfacial Magnetism Measured by Using a Scanning Tunneling Microscope Tip, *Appl. Phys. Lett.*, 2018, **113**(6), 1–6, DOI: 10.1063/1.5031877.

19 L. E. Fuentes-Cobas, M. E. Montero-Cabrera, L. Pardo and L. Fuentes-Montero, *Ferroelectrics under the Synchrotron Light: A Review*; 2016, vol. 9. DOI: 10.3390/ma9010014.

20 L. Fleming, C. C. Fulton, G. Lucovsky, J. E. Rowe, M. D. Ulrich and J. Lüning, Local Bonding Analysis of the Valence and Conduction Band Features of TiO2, *J. Appl. Phys.*, 2007, **102**(3), 033707-1–033707-7, DOI: 10.1063/1.2764004.

21 Z. Wu, F. Langenhorst, F. Seifert, E. Paris and A. Marcelli, Oxygen 1s ELNES Study of Perovskites (Ca,Sr,Ba)TiO3, *J. Synchrotron Radiat.*, 2001, **8**(2), 934–936, DOI: 10.1107/S0909049500020653.

22 O. Kamon-In, W. Pattanasiriwisawa, A. Yangthaisong and S. Srilomsak, Structural Studies of Ba1-XLaxTiO3 Using X-Ray Absorption near-Edge Spectroscopy, *J. Phys.: Conf. Ser.*, 2009, **190**(1), 012082, DOI: 10.1088/1742-6596/190/1/012082.

23 J. J. Kas, J. Vinson, N. Trcera, D. Cabaret, E. L. Shirley and J. J. Rehr, Many-Pole Model of Inelastic Losses Applied to Calculations of XANES, *J. Phys.: Conf. Ser.*, 2009, **190**(1), 012009, DOI: 10.1088/1742-6596/190/1/012009.

24 J. Vinson, J. J. Rehr, J. J. Kas and E. L. Shirley, Bethe-Salpeter Equation Calculations of Core Excitation Spectra, *Phys. Rev. B: Condens. Matter Mater. Phys.*, 2011, **83**(11), 115106, DOI: 10.1103/PhysRevB.83.115106.

25 F. M. F. de Groot, H. Elnaggar, F. Frati, R. p. Wang, M. U. Delgado-Jaime, M. van Veenendaal, J. Fernandez-Rodriguez, M. W. Haverkort, R. J. Green, G. van der Laan, Y. Kvashnin, A. Hariki, H. Ikeno, H. Ramanantoanina, C. Daul, B. Delley, M. Odelius, M. Lundberg, O. Kuhn, S. I. Bokarev, E. Shirley, J. Vinson, K. Gilmore, M. Stener, G. Fronzoni, P. Decleva, P. Kruger, M. Retegan, Y. Joly, C. Vorwerk, C. Draxl, J. Rehr and A. Tanaka, 2P X-Ray Absorption Spectroscopy of 3D Transition Metal Systems, *J. Electron Spectrosc. Relat. Phenom.*, 2021, **249**, 147061, DOI: 10.1016/j.elspec.2021.147061.

26 I. Tanaka, T. Mizoguchi and T. Yamamoto, XANES and ELNES in Ceramic Science, *J. Am. Ceram. Soc.*, 2005, **88**(8), 2013–2029, DOI: 10.1111/j.1551-2916.2005.00547.x.

27 A. P. Grosvenor, M. C. Biesinger, R. S. C. Smart and N. S. McIntyre, New Interpretations of XPS Spectra of Nickel Metal and Oxides, *Surf. Sci.*, 2006, **600**(9), 1771–1779, DOI: 10.1016/j.susc.2006.01.041.

28 C. A. Ullrich and Z. h. Yang, A Brief Compendium of Time-Dependent Density Functional Theory, *Braz. J. Phys.*, 2014, **44**, 154–188, DOI: 10.1007/s13538-013-0141-2.

29 C. D. Pemmaraju, Simulation of Attosecond Transient Soft X-Ray Absorption in Solids Using Generalized Kohn-Sham Real-Time Time-Dependent Density Functional Theory, *New J. Phys.*, 2020, **22**(8), 083063, DOI: 10.1088/1367-2630/aba76c.

30 A. Di Cicco, Local, Structure in Molecular Complexes Probed by Multiple-Scattering XAS, *J. Synchrotron Radiat.*, 2003, **10**(1), 46–50, DOI: 10.1107/S0909049502017193.

31 Z. Wu, G. Ouvrard and P. Gressier, Ti and O K Edges for Titanium Oxides by Multiple Scattering Calculations: Comparison to XAS and EELS Spectra, *Phys. Rev. B: Condens. Matter Mater. Phys.*, 1997, **55**(16), 10382, DOI: 10.1103/PhysRevB.55.10382.

32 A. Filipponi and A. Di Cicco, Gnxas: A Software Package for Advanced Exafs Multiple-Scattering Calculations and Data-Analysis, *Task Q*, 2000.

33 T. Nakamura, R. Oike, Y. Kimura, Y. Tamenori, T. Kawada and K. Amezawa, Operando Soft X-Ray Absorption Spectroscopic Study on a Solid Oxide Fuel Cell Cathode during Electrochemical Oxygen Reduction, *ChemSusChem*, 2017, **10**(9), 2008–2014, DOI: 10.1002/cssc.201700237.

34 Y. Liang, J. Vinson, S. Pemmaraju, W. S. Drisdell, E. L. Shirley and D. Prendergast, Accurate X-Ray Spectral Predictions: An Advanced Self-Consistent-Field Approach Inspired by Many-Body Perturbation Theory, *Phys. Rev. Lett.*, 2017, **118**(9), 096402, DOI: 10.1103/PhysRevLett.118.096402.

35 K. Gilmore, J. Vinson, E. L. Shirley, D. Prendergast, C. D. Pemmaraju, J. J. Kas, F. D. Vila and J. J. Rehr, Efficient Implementation of Core-Excitation Bethe-Salpeter Equation Calculations, *Comput. Phys. Commun.*, 2015, **197**, 109–117, DOI: 10.1016/j.cpc.2015.08.014.

36 P. Abbasi, N. Shirato, R. E. Kumar, I. V. Albelo, M. R. Barone, D. N. Cakan, M. d. l. P. Cruz-Jáuregui, S. Wieghold, D. G. Schlom, V. Rose, T. A. Pascal and D. P. Fenning, Nanoscale Surface Structure of Nanometer-Thick Ferroelectric BaTiO 3 Films Revealed by Synchrotron X-Ray Scanning Tunneling Microscopy: Implications for Catalytic Adsorption Reactions, *ACS Appl. Nano Mater.*, 2023, **6**(3), 2162–2170, DOI: 10.1021/acsanm.2c05257.

37 J. Torgersen, S. Acharya, A. L. Dadlani, I. Petousis, Y. Kim, O. Trejo, D. Nordlund and F. B. Prinz, Relating Electronic and Geometric Structure of Atomic Layer Deposited BaTiO3 to Its Electrical Properties, *J. Phys. Chem. Lett.*, 2016, **7**(8), 1428–1433, DOI: 10.1021/acs.jpclett.6b00393.

38 M. Bugnet, G. Radtke, S. Y. Woo, G. Z. Zhu and G. A. Botton, Temperature-Dependent High Energy-Resolution EELS of Ferroelectric and Paraelectric BaTiO3 Phases, *Phys. Rev. B*, 2016, **93**(2), 1–5, DOI: **10.1103/PhysRevB.93.020102**.

39 N. Shirato, M. Cummings, H. Kersell, Y. Li, B. Stripe, D. Rosenmann, S.-W. Hla and V. Rose, Elemental Fingerprinting of Materials with Sensitivity at the Atomic Limit, *Nano Lett.*, 2014, **14**(11), 6499–6504, DOI: **10.1021/nl5030613**.

40 V. Rose, T. Ajayi, D. Rosenmann and N. Shirato, A Variable X-Ray Chopper System for Phase-Sensitive Detection in Synchrotron X-Ray Scanning Tunneling Microscopy, *J. Synchrotron Radiat.*, 2020, **27**(5), 1382–1387, DOI: **10.1107/S1600577520007869**.

41 V. Rose, K. Wang, T. Chien, J. Hiller, D. Rosenmann, J. W. Freeland, C. Preissner and S. W. Hla, Synchrotron X-Ray Scanning Tunneling Microscopy: Fingerprinting near to Far Field Transitions on Cu(111) Induced by Synchrotron Radiation, *Adv. Funct. Mater.*, 2013, **23**(20), 2646–2652, DOI: **10.1002/adfm.201203431**.

42 F. de Groot and A. Kotani, *Core Level Spectroscopy of Solids*; 2008. DOI: **10.1201/9781420008425**.

